Materialia 26 (2022) 101558

Contents lists available at ScienceDirect

Materialia

journal homepage: www.elsevier.com/locate/mtla

Full Length Article

Germanium electrodeposition into porous silicon for silicon-germanium alloying

Nikita Grevtsov [a,*], Eugene Chubenko [a], Vitaly Bondarenko [a], Ilya Gavrilin [b], Alexey Dronov [b], Sergey Gavrilov [b]

[a] *Belarusian State University of Informatics and Radioelectronics, Minsk, Belarus*
[b] *National Research University of Electronic Technology, Zelenograd, Moscow, Russia*

ARTICLE INFO

Keywords:
Electrodeposition
Porous silicon
Germanium
Silicon-germanium alloys

ABSTRACT

A method of germanium electrodeposition from a GeO_2-based aqueous solution into the pore channels of anodic mesoporous silicon formed on n-type highly-doped (100) silicon wafers is described. The effect of deposition time, pore channel shape and preconditioning of porous silicon layers in hydrofluoric acid is evaluated. Recommendations are given in regards to the optimal parameter combinations to ensure uniform pore channel filling with germanium. The possibility of producing silicon-germanium alloys by subsequent rapid heat treatment of the germanium-filled porous silicon layers is established.

1. Introduction

Composite semiconductor structures based on silicon and germanium are currently of prominent interest as a structural basis for producing silicon-germanium alloys of various compositions (e.g., $Si_{0.8}Ge_{0.2}$), which are most notable for their outstanding thermoelectric properties [1]. The currently employed approaches to the production of Si-Ge alloys are fairly complicated and generally require expensive equipment and complex technological processes such as epitaxy and hot pressing, as well as rely on toxic and/or flammable germanium precursors [2]. Alternative methods have also been proposed, such as the one by Volodin et. al., involving nano-, pico- and femtosecond infrared pulsed laser annealing of multilayer structures consisting of alternating thin films of amorphous silicon and germanium; however, only picosecond laser annealing proved effective, and only thin nanoscale SiGe layers could be produced [3]. In this regard, finding alternative more simplistic and flexible ways to form alloy layers of ample thicknesses remains an urgent task. Electrochemical deposition of germanium into porous silicon (PS) – a material obtained by electrochemical or chemical etching of monocrystalline silicon in hydrofluoric acid-based solutions – stands out as a potential candidate for such a role. Presumably, thermal treatment of PS with its pore channels filled with germanium at temperatures above the latter's melting point will enable acquisition of Si-Ge alloys. The ensuing alloy layer's thickness will then mainly be determined by that of the initial PS layer, and its composition – by PS's structural parameters and the pore filling factor.

Electrochemical deposition from liquid solutions is well-regarded as an effective approach to produce germanium films on conducting and semiconducting substrates. Among the most popular sources of germanium ions for its electrochemical reduction are solutions based on germanium chloride $GeCl_4$. The less common alternatives include but are not limited to germanium's halogen salts ($GeBr_4$, GeI_4) and germanium dioxide GeO_2. Molten salts and ionic liquids are most often used as solvents, as they are generally known to provide the largest electrochemical window. Lahiri et al. describe the possibility of germanium plating from GeX_4 (where X = Cl, Br, I) dissolved in an ionic liquid ($[BMIm]PF_6$) and note a strong effect of UV illumination on the reduction potential [4]. Processes of this kind can be realized at room temperature [5] and are characterized by two-step reduction of germanium ($Ge^{4+} \rightarrow Ge^{2+} \rightarrow Ge^{0}$) [6]. Raising the temperature leads to higher deposition rates due to an increase in the electrical conductivity of the resulting films, as well as the acceleration of overall electrochemical kinetics [7]. Germanium reduction from solutions based on ionic liquids and high-temperature molten salts allows the formation of germanium structures (e.g., nanoscale filaments) that exhibit satisfactory structural parameters and cyclic strength for use as lithium-ion battery anodes [5,8,9].

Reduction from aqueous solutions is the least common group of electrochemical approaches to obtaining crystalline germanium. This can mostly be attributed to germanium's tendency to oxidize in the presence of water, as well a rather minor electrochemical window due to the small hydrogen evolution overpotential, making it harder to obtain thicker layers [7]. Fink and Dokras described the basic process of germa-

* Corresponding author.
E-mail address: hrautsou@gmail.com (N. Grevtsov).

https://doi.org/10.1016/j.mtla.2022.101558
Received 5 July 2022; Accepted 27 August 2022
2589-1529/© 2022 Acta Materialia Inc. Published by Elsevier B.V. All rights reserved.

nium deposition from aqueous solutions based on $GeCl_4$ [10]. Among more recent works, Liang et al. have evaluated the deposition process from solutions based on germanium chloride using cyclic voltammetry, establishing that monolayer germanium can be deposited on a noble metal substrate, and the reduction process itself occurs over several stages ($Ge^{4+} \rightarrow GeOH_{(ads.)} \rightarrow GeH_{(ads.)}$) [11]. Among other possible solvents providing favorable conditions for germanium reduction, organic substances such as ethylenediamine [12], supercritical fluids based on CO_2 [13] and difluoromethane [14], as well as propylene glycol [15,16] are noted. Approaches based on these solvents have a number of advantages, but can be difficult to implement in practice due to the need to completely eliminate the presence of water.

It is important to note that the works listed above, with few exceptions, are devoted to the deposition of germanium onto flat conducting substrates. Recovery of crystalline germanium on semiconductor materials, especially nanostructured ones, is much less explored. It has been established that, to form germanium crystallites on a silicon substrate, predeposited particles of fusible metals (In, Ga) or alloys (GaIn, BiIn) can be utilized. In that case, germanium can be deposited using the so-called electrochemical liquid-liquid-solid (ec-LLS) growth approach, which implies electrolysis of this fusible metal-covered semiconductor substrate in GeO_2-based solutions [17,18] During ec-LLS metal particles take on two primary roles, serving as (a) microscopic cathodes whereon oxidized germanium is reduced to its atomic state, as well as (b) the medium for nucleation and growth of the forming semiconductor crystallites. The result is the growth of germanium in the form of thin wire-like filaments which correlate in diameters with the original metal particles. The disadvantage of this approach is the presence of residual fusible metal contents in the composites, as well as (in cases when high temperatures are utilized) relatively poor reproducibility. As we have previously assumed [19], the ec-LLS process can be carried out on PS which had its pores filled with fusible metal particles in advance, enabling selective growth of germanium crystallites inside the pores. Heat treatment of the resulting structures leads to the formation of $Si_{1-x}Ge_x$ alloys with high germanium contents [20]. It is important to note that filling microscopic pore channels with other substances is not an easy task, and so far, the possibility of doing so has only been demonstrated for a select few metals. The greatest success has been achieved with nickel, cobalt, iron, and copper, while conformal deposition with reproducible filling of each consecutive pore has only been realized for nickel [21].

The purpose of the present work is to investigate the electrochemical deposition of germanium into PS layers without any preliminarily deposited fusible metal coverage, evaluating the influence of a number of technological parameters on the morphology of the obtained deposit and its potential usability as a basis for silicon-germanium alloying.

2. Materials and methods

PS layers used as matrices for subsequent filling with germanium were obtained by electrochemical anodization of antimony-doped (100)-oriented monocrystalline silicon wafers with a bulk resistivity of 0.01 Ohm·cm. The diameter and thickness of the wafers used were 100 mm and 460 μm, respectively. All the necessary electrochemical treatment stages were performed using a Metrohm Autolab PGSTAT302N potentiostat under room illumination.

To obtain PS layers, initial monocrystalline silicon wafers were divided into rectangular samples about 4 cm^2 in area. Each sample was rinsed with deionized water and air-dried in-between each of the following processing stages, unless specified otherwise. Firstly, the samples were cleaned of organic contaminants in chromic acid, then immersed into a 5% HF solution for oxide removal. For electrochemical anodization, each sample was treated in an electrochemical cell with a circular working area 1.9 cm in diameter. The electrolyte used for the anodization process consisted of 1 volume part 45% hydrofluoric acid HF, 3 parts deionized water and 1 part isopropyl alcohol. Mesoporous silicon layers approximately 1.5 μm thick were obtained by anodizing the sample at a current density of 70 mA/cm^2 for 30 s.

Due to the specifics of PS formation, its subsurface layer is characterized by significantly smaller pore sizes. To eliminate any possible negative effect of this occurrence on germanium deposition, the subsurface layer was removed by a two-stage chemical etching procedure. The first stage involved chemical (immersion) deposition of copper into the subsurface layer from an aqueous solution containing 0.03 M $CuSO_4$ and 0.14 M HF for 3 min. This results in silicon's chemical dissolution and displacement of its atoms with those of copper [22]. In the case of porous silicon, this process is generally contained in its subsurface area due to significant diffusion limitations, as well as the presence of large amounts of structural defects, and the rest of the layer remains mostly intact. On the second stage, the previously deposited metal was etched in a 20% HNO_3 solution for 5 min, which simultaneously resulted in the removal of the subsurface layer displaced by copper atoms. Since nitric acid leads to silicon's oxidation, each PS sample was additionally immersed in concentrated hydrofluoric acid to remove the oxide layer before proceeding with germanium deposition. This procedure was executed out for a relatively long period of time (1 h) to take into account the capillary effects that slow down the the acid's access into the lower ends of the pore channels.

An aqueous solution containing 0.05 M GeO_2, 0.5 M K_2SO_4 and 0.1 M $C_4H_5O_4$ (succinic acid) with pH adjusted to 6.5 using NH_4OH was used for germanium deposition. The process was carried out for 30 min with vertical electrode arrangement in galvanostatic mode at a current density of 2 mA/cm^2 and solution temperature of 85 ^{0}C, maintained by a laboratory heating plate IKA C-MAG HS 7. In order to obtain an alloy layer, germanium-filled PS was subjected to rapid thermal processing (RTP) using an Annealsys As-One 100 RTP system. Thermal processing was conducted at 950 °C over the course of 30 s under argon flow (800 sccm). This temperature value is above germanium's melting point, leading to the latter's alloying with PS's sidewalls. Naturally, the alloyed film's thickness is expected to be equal to or lower than that of the initial porous layer.

Fig. 1 shows a generalized schematic illustration of the proposed technological approach to the fabrication of Si-Ge composites and alloys, including PS preparation, germanium deposition and silicon-germanium alloying.

The samples' structural parameters were studied using a Hitachi S-4800 scanning electron microscope (SEM). The diameter of the electron beam was 1 nm. The samples' elemental composition (namely, distribution profiles and concentration mapping of chemical elements present along the porous layer's thickness) was evaluated by means of energy dispersive X-ray spectroscopy (EDX) using a Bruker QUANTAX 200 spectrometer. The method in question relies on scanning the electron beam over the sample's cross-section and recording the X-ray spectra from excitation areas with diameters not exceeding 0.5 μm at an accelerating voltage of 15 kV. Since the sizes of structural elements under evaluation generally lie well below this value, the obtained concentration values can be interpreted as average throughout said excitation area, and the elemental distribution profiles and EDX maps based thereon are therefore presented in relative units. Since the spectra acquisition conditions remained the same for all the samples in this work, we consider this approach valid for the sake of comparison.

In addition to EDS, a 3D scanning laser confocal Raman microscope Confotec® NR500 equipped with a 473 nm blue laser was used to analyze the surface layer's composition. This was especially practical for the basic detection of Si-Ge alloying achieved via RTP.

Surface SEM images of initial PS layers were analyzed using ImageJ software, enabling the calculation of the cross-sectional area S for each of the pores present in the image. The equivalent pore diameter D_{eq} is then calculated as the diameter of a circle possessing the same area as the pore: $D_{eq} = 2 \bullet (S/\pi)^{1/2}$.

The pore sidewall thickness was estimated in a similar fashion using an ImageJ expansion created by Haeri and Haeri [23], wherein the dis-

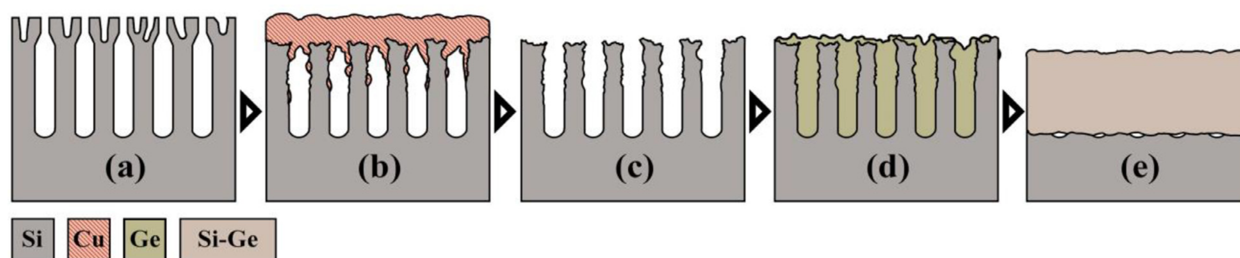

Fig. 1. Schematic illustration of the proposed silicon/germanium composite formation method: (a) initial PS layer, (b) Cu deposition into the subsurface layer, (c) subsurface layer removal in HNO_3 and HF immersion for oxide removal, (d) germanium deposition (e) thermal processing for alloy formation.

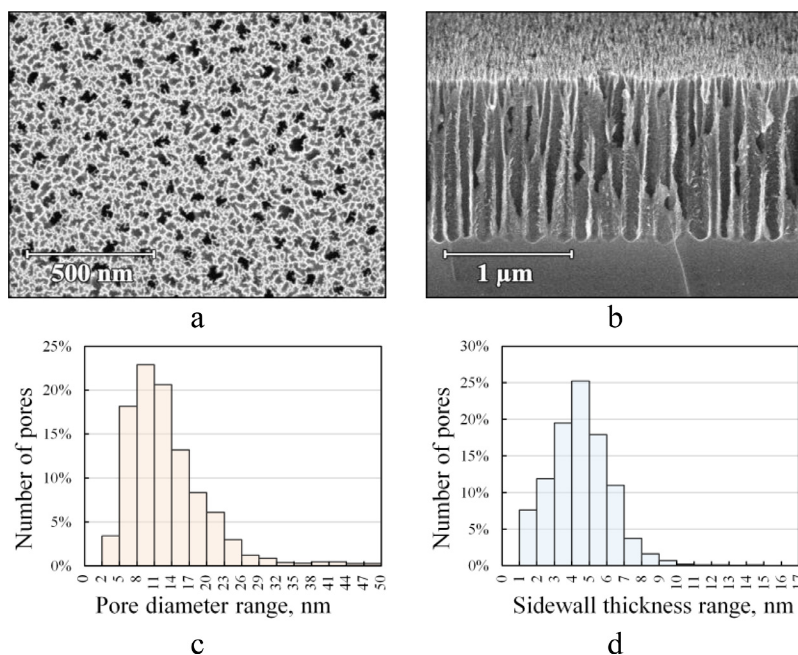

Fig. 2. SEM images of (a) surface, (b) cross-section and histograms of (c) equivalent pore diameter and (d) pore sidewall thickness distribution for the freshly-prepared PS with its subsurface layer still intact.

tance d between the boundaries of two adjacent pores with coordinates x_1, y_1 and x_2, y_2 is determined as $d = 2\bullet((y_2 - y_1)^2 + (x_2 - x_1)^2)^{1/2} - (r_1 + r_2)$, where r_1 and r_2 are the equivalent radii of two pores calculated from their areas under assumption that they have a circular shape. Considering the pore shape approximation, this method gives the most accurate results for circular pores, but is sufficiently applicable to the structures considered in this paper.

3. Results

3.1. Effect of porous silicon's subsurface layer

Fig. 2 shows surface and cross-section SEM images of a freshly prepared PS sample, as well as histograms demonstrating statistical distribution of pore diameters and sidewall thicknesses. The surface pore density in this case is $2.04 \cdot 10^{11}$ cm^{-2}, and the pores' equivalent diameters range from 3 to 52 nm with an average value of 17 nm. Most of the pores are gray in color, indicating their shallow depth, but black pores are also present and are generally larger in lateral size. The sidewall thickness value ranges from 1 to 15 nm, with an average of 5 nm. The PS layer is about 1.5 μm thick, with pore channels exhibiting a characteristic bottle-like shape with noticeable topside tapering and a well-developed surface with a large total area. The subsurface layer with reduced pore sizes is around 0.3 um in thickness. The primary pore channels are directed strictly perpendicular to the wafer's surface.

In order to assess the subsurface layer's effect on deposit localization, deposition of germanium into freshly-prepared PS samples with the layer in question still intact was first evaluated. The sample was preliminarily immersed in concentrated HF for 30 min, whereafter the deposition process was carried out over the course of 30 min. Fig. 3 shows the SEM images of the resulting structure. Here we also present the EDX analysis results in the form of EDX mapping data and element concentration profiles (for silicon, germanium and oxygen) in relation to the pore channel depth, with 0% being the upper edge of the layer and 100% corresponding to the PS/monocrystalline Si boundary. The scan was performed at a 45° angle relative to the samples' surface to ensure more representative results.

Fig. 3a and b clearly indicate that the subsurface region of the sample is entirely coated by a dense germanium film. It would be logical to assume that this sort of pore "clogging" is primarily caused by their small lateral size and leads to considerable diffusion limitations. This provides less than favorable conditions for deep germanium plating, which is evident from EDX concentration profiles. The latter would indicate that germanium is predominantly located on the surface and in the subsurface layers of PS, and its concentration noticeably decreases along with the pore depth. An exponential increase in silicon's concentration after a depth threshold of 60% is most likely caused by an integral character of the EDX technique, manifested in the electron beam starting to partially capture the signal from the monocrystalline wafer below the porous layer.

Considering the noticeable pore clogging and an excessive deposit gradient all throughout the porous layer, all the following studies were carried out on PS samples with their subsurface layers removed. The SEM images and corresponding statistical distributions of the pores' ge-

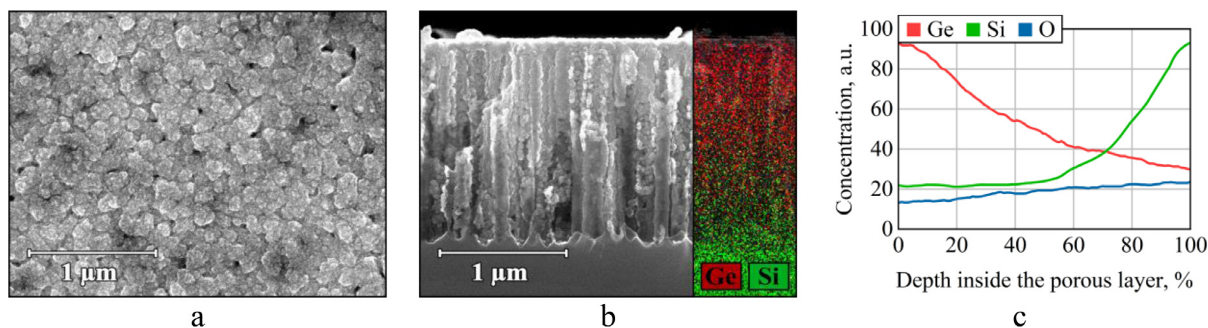

Fig. 3. SEM images of (a) surface, (b) cross-section (with EDX signature map overlaid over the right-hand side), and (c) EDX distribution profiles of Si and Ge in a sample prepared by depositing germanium into freshly-prepared PS with its subsurface layer still intact at a current density of 2 mA/cm^2 for 30 min. The PS sample was preconditioned in HF for 60 min.

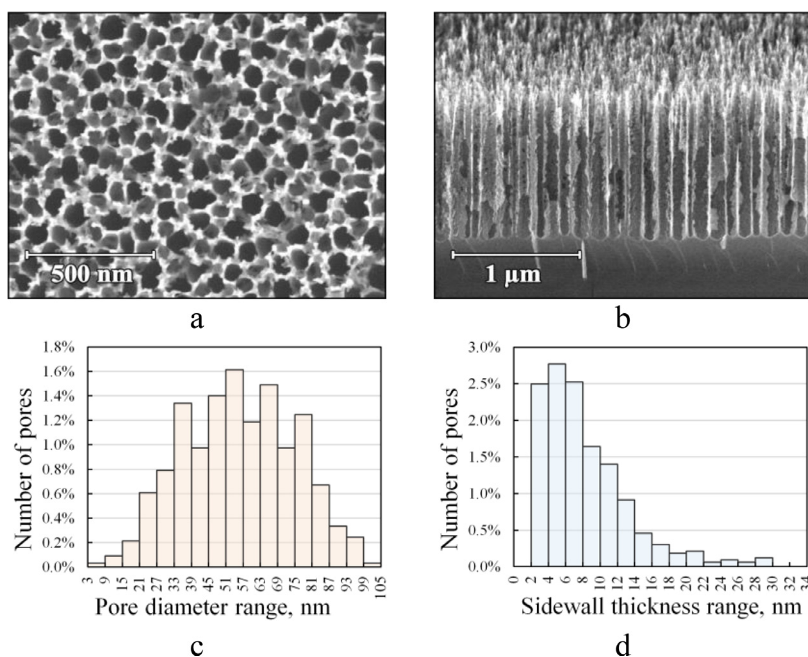

Fig. 4. SEM images of (a) surface, (b) cross-section and histograms of (c) equivalent pore diameter and (d) pore sidewall thickness distribution for the PS layer with its subsurface layer chemically removed.

ometrical parameters for one such sample are compiled in Fig. 4. In this case, the pores have pronounced cylindrical shapes without the characteristic topside tapering. Due to the etching mechanism involving silicon atoms' replacement with copper atoms and subsequent dissolution of the latter, the remnants of the etched subsurface layer have a well-developed rough nature. The pores on the surface possess equivalent diameters ranging from 4 to 102 nm with an average value of 56 nm – around three times larger than that in freshly prepared PS. The pore placement density is $5.32{\cdot}10^9$ cm^{-2}, which is almost two orders of magnitude lower than that in the subsurface layer. Lastly, the sidewall thickness ranges from 3 to 30 nm with an average value of 9 nm, compared to 5 nm in the initial porous layer.

3.2. Effect of deposition time

SEM images and EDX data for PS samples with germanium deposits obtained after 10-, 20-, 30- and 40 min deposition processes are compiled in Fig. 5. Each sample had its subsurface layer chemically removed and was pre-conditioned in concentrated hydrofluoric acid for 1 h. The feasibility of such a preconditioning procedure will be demonstrated in the following section.

The obtained data seem to indicate that germanium nucleation occurs at select points on the sidewall surface. These nuclei then proceed to increase in size over time and soon coalesce into a continuous germanium "column", whose growth is confined in a vertical direction by the pore channel boundaries. The result is a sufficiently uniform degree of pore filling with germanium, which, however, does not exclude the formation of a noticeable germanium layer on the surface. A value of 30 min was chosen as the optimal time interval to ensure complete filling of the pores, while also avoiding excessive surface precipitation that occurs at prolonged electrolysis durations. This deposition time was therefore used in all subsequent studies.

3.3. Effect of preliminary exposure to HF

To evaluate the effect of PS layer preconditioning in hydrofluoric acid, we varied the samples' immersion time in HF and evaluated its effect on the germanium deposit. The corresponding results are presented in Fig. 6.

While noticeable negative effects are present in the case of insufficient HF exposure, any change in the procedure's duration after the sample has already been subjected to prolonged immersion does not seem to result in any significant changes in the deposit's morphology. The implications of this phenomenon will be discussed further.

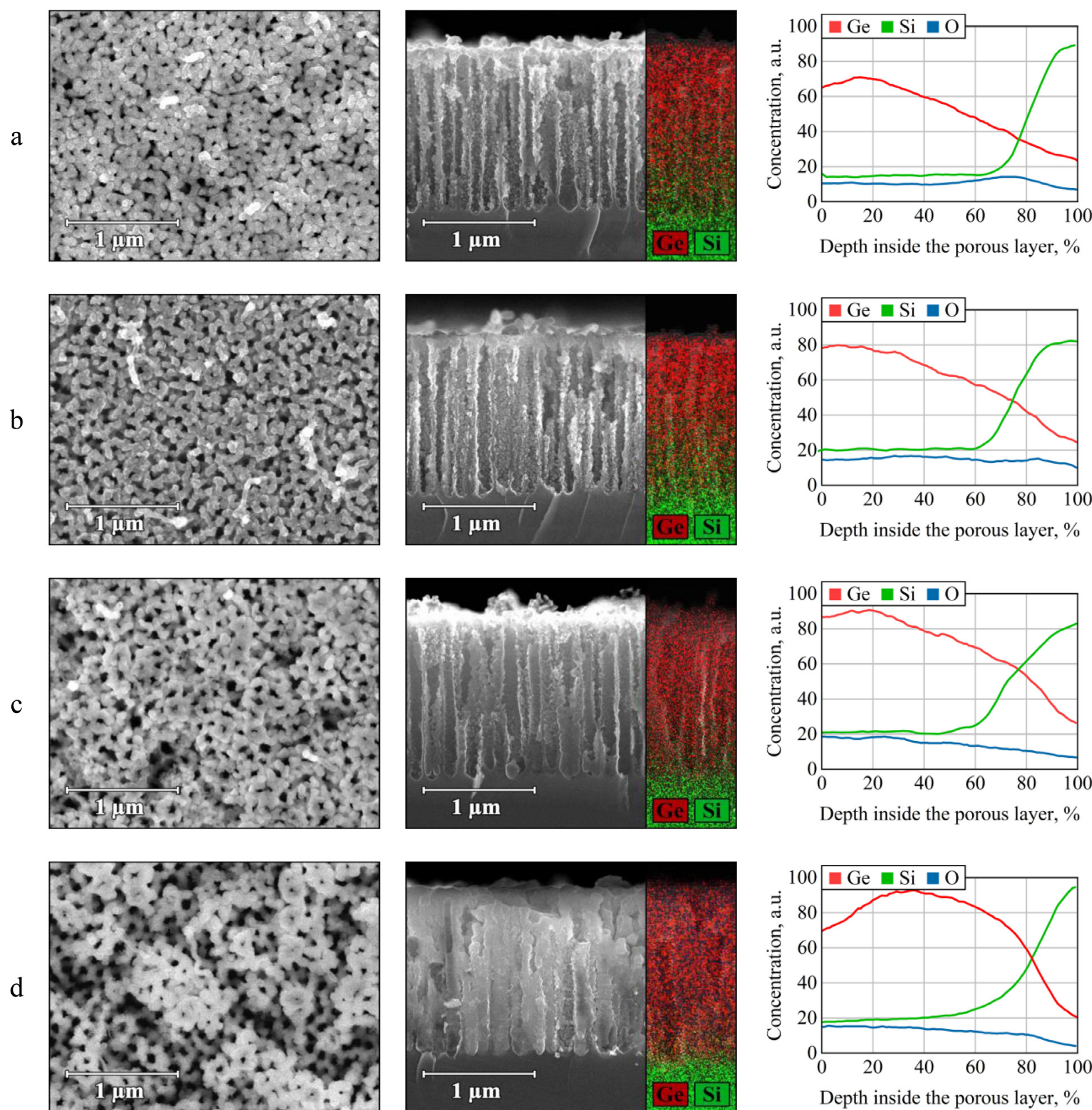

Fig. 5. Surface/cross-section SEM images (with EDX signature maps overlaid over the right-hand sides) and EDX distribution profiles of Si and Ge in PS samples with germanium deposited at current density of 2 mA/cm^2 for (a) 10 min, (b) 20 min, (c) 30 min, (d) 40 min. Each PS sample had its subsurface layer removed and was preconditioned in HF for 60 min.

3.4. Thermal processing for Si-Ge alloy formation

Figs. 7 and 8 compile the SEM images and Raman spectra of the Si-Ge alloy layer produced via RTP of the silicon/germanium composite obtained in accordance with the previously described approach comprising a 60 min HF preprocessing stage and a 30 min germanium deposition stage (similarly to Figs. 5c and 6b). The comparison of Raman spectra illustrating the difference between the samples' composition before and after thermal processing is shown in Fig. 8.

As seen from Fig. 7, stemming from RTP is a uniform alloyed layer around 500 nm in thickness, which is substantially thinner compared to the original 1.5 μm thick PS used for its acquisition. Amid the smooth alloy droplets up to a few micrometers in size some inconsistencies are present in the form of nanoscale crystallites. This kind of irregular shape is most likely associated with germanium being present on top of the PS layer before the thermal processing is initiated and can likely be solved by adjusting the germanium deposition parameters to minimize surface nucleation.

As the goal of the present work is to simply establish the possibility of producing Si-Ge alloys through this approach, the effect of all the processing parameters listed above on the alloy's morphology and composition is yet unclear and is to be determined in future research. The discussion section will therefore be focused solely on germanium deposition.

4. Discussion

Fig. 9 illustrates the nucleation and growth stages of germanium crystallites within the pores, based on the SEM images presented earlier. It also includes the case when the PS layer in question still has its subsur-

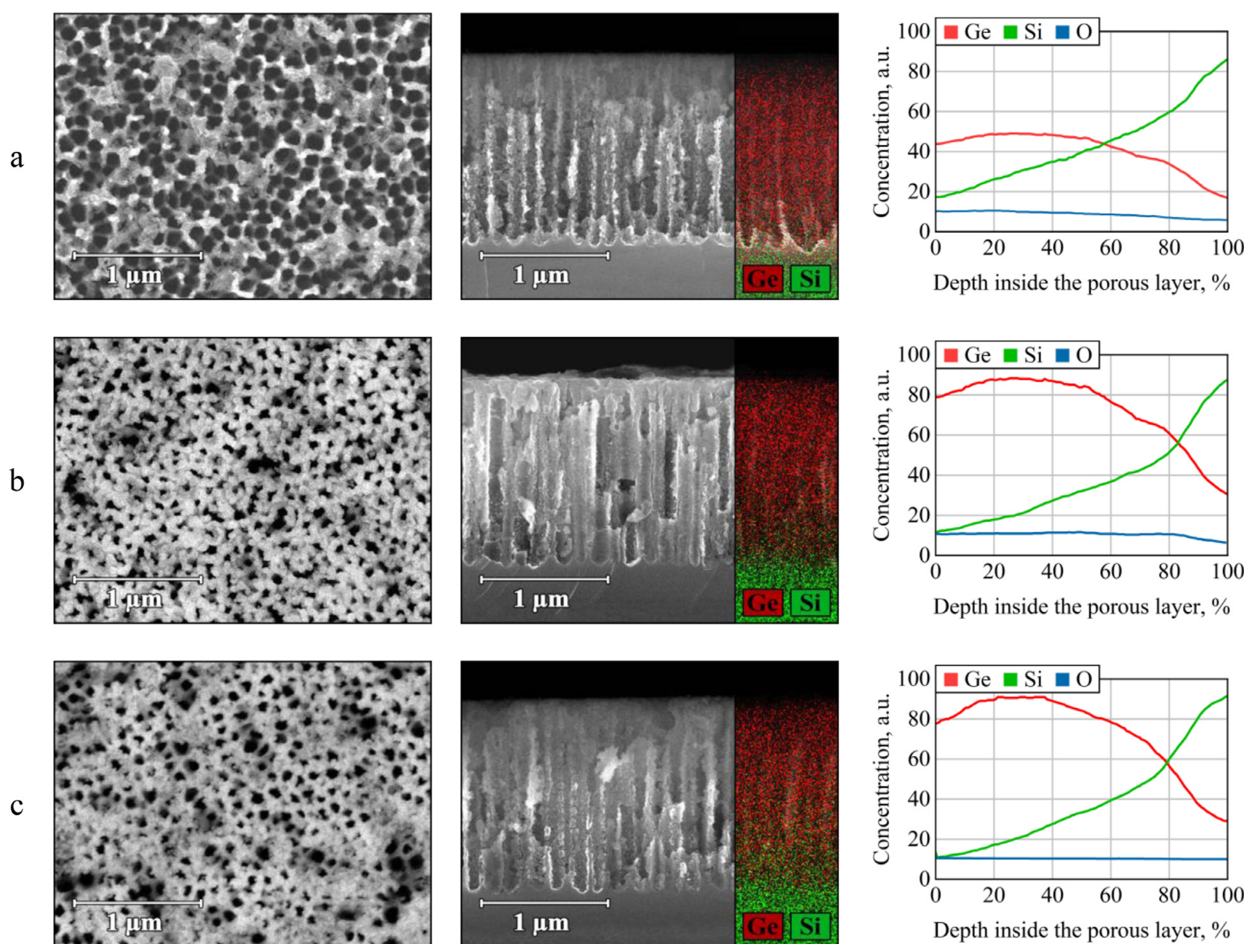

Fig. 6. Surface/cross-section SEM images (with EDX signature maps overlaid over the right-hand sides) and EDX distribution profiles of Si and Ge in PS samples with germanium deposited at a current density of 2 mA/cm^2 for 30 min. The samples had their subsurface layers removed and were preconditioned in HF for (a) 30 s, (b) 30 min and (c) 60 min.

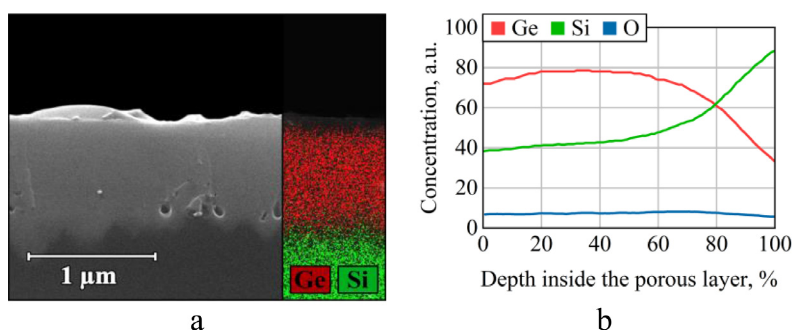

Fig. 7. (a) Cross-section SEM image (with EDX signature map overlaid over the right-hand side) and (b) EDX distribution profiles a of Si-Ge alloy layer produced by RTP (950 °C, 30 s) of PS electrochemically filled with germanium at 2 mA/cm^2 for 30 min.

face layer intact. At the early stages of the process (Fig. 4, a) germanium growth in the form of spherical particles with diameters ranging from 50 to 150 nm can be observed. Judging from SEM data, the particles' spatial packing density (under the assumption that the horizontal N_x and vertical N_y packing densities are equal) is roughly equal to $N = N_x \cdot N_y \approx 9.6 \cdot 10^9$ cm^{-2}. As the electrolysis process goes on, the particles increase in number and size, gradually coalescing into one another and soon completely enveloping the surface of the pore. At a certain point the gap between the sidewalls encloses, yielding a pore fully-filled with germanium. It is worth noting that the solution's renewal may be drastically hindered by the gradually decreasing gap between the sidewalls, making it more likely for the subsurface areas to enclose first, bringing about underlying cavities inside the deposit. While this factor is especially prevalent in freshly-prepared PS layers with the subsurface layer still intact, we do not expect it to have any serious negative impact on alloy formation in the case of preprocessed PS with the subsurface layer removed.

The seemingly substantial effect of PS preconditioning by HF immersion prior to germanium deposition can be attributed to at least two factors.

Firstly, by exposing the sample to hydrofluoric acid, which easily dissolves SiO_2, it is possible to minimize the negative effect of the natural oxide film that forms both due to the aqueous nature of the solutions used and due to surface's previous exposure to nitric acid. This eliminates the need for electrical breakdown of the oxide layer for germanium nucleation, or greatly facilitates it, thereby increasing nucleation den-

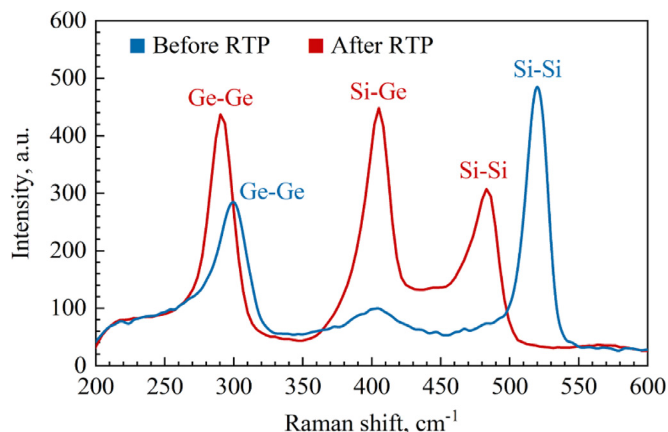

Fig. 8. Raman spectra comparison for PS samples with germanium electrodeposited at a current density of 2 mA/cm^2 for 30 min before and after rapid thermal processing.

sity. Nevertheless, one should also expect that the consequent increase in the hydrophobicity of the pore sidewall surface will lead to some deterioration in the wettability of the latter, complicating solution flow deeper into the pores. The ratio between negative and positive effects of this factor remains uncertain.

Secondly, exposure to HF or its aqueous solutions for sufficiently long periods of time leads to hydrogen termination of the pore sidewalls. The importance of this procedure in terms of silicon surface functionalization has been previously considered in the works of J. Buriak et al. and other authors [24]. In particular, the presence of Si-H bonds on the surface presents favorable conditions for metal nucleation and growth compared to surface passivation by SiO_2, since it provides increased surface reactivity, with the hydrogen atoms being able to more easily get replaced by atoms of the reduced material [25]. In addition to that, hydrogen passivation makes the surface more chemically homogeneous and, in the short term, stable to oxidation in an air atmosphere [23,26]. At the same time, it is to be expected that some of the Si-H bonds may undergo oxidation in aqueous solutions, and different segments of the surface may not be equally functionalized [27].

The nature of the silicon surface termination by SiH_x groups depends on the crystallographic orientation of the surface in question. In the case of PS, which can have surfaces with various orientations, different kinds of bonds are expected to occur in its different regions: surfaces corresponding to the (100) direction are covered by dimeric monohydrides or dihydrides; those with a (111) direction are terminated by isolated Si-H groups; finally, SiH_3 trihydrides can exist on highly defective surfaces such as the well-developed upper part of the porous layer [28,29]. Additionally, diffusion of hydrogen into the crystal lattice of silicon may create electronic states in the band gap [30], which also contributes to the overall positive beneficial effect.

It should be noted that carrying out the same deposition process on a monocrystalline wafer of the same type results in small-scale deposits separated into individual spots and conglomerations that do not cover the entire surface of the sample. The germanium deposits in question do not produce any signatures on the Raman shift measurements, indicating their insufficient amounts. Evidently, PS significantly promotes germanium nucleation density due to its well-developed surface with numerous defects and other potential nucleation points throughout. It also prevents the resulting nuclei and germanium crystallites from being washed away by the flow of water used for rinsing the sample after the procedure is concluded.

5. Conclusions

The obtained results indicate that compliance with a set of processing parameters during electrochemical deposition of germanium into PS from aqueous solutions based on GeO_2 makes it possible to achieve uniform and reproducible filling of pores with germanium. The germanium deposits obtained by such an approach have the shape of scattered germanium clusters, which increase in size and gradually and reproducibly fill the pore channels as the electrolysis duration is increased.

The subsurface layer that is typically present in mesoporous silicon layers and features pores of smaller diameters plays a crucial role in deposit localization. Removing it by chemically displacing it with copper and etching it in nitric acid greatly improves the pore filling factor by

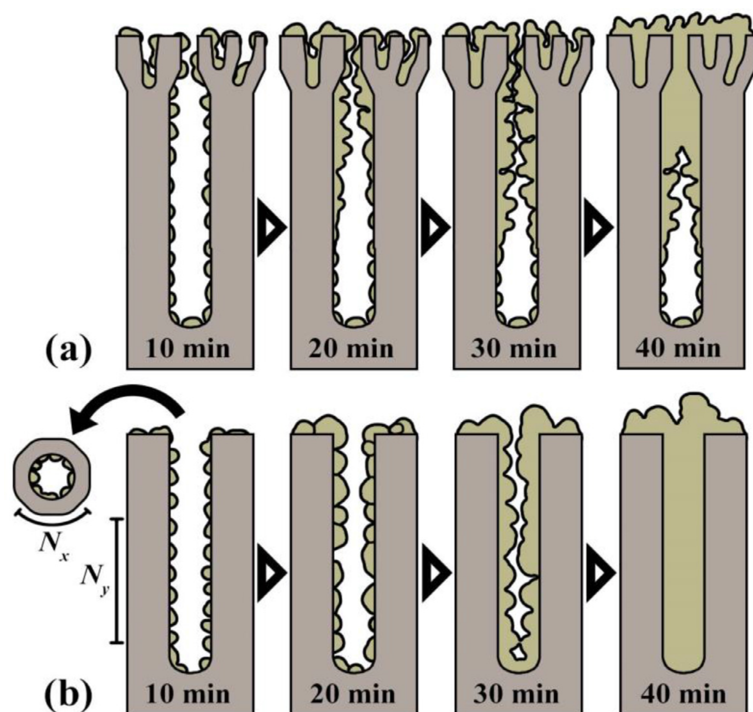

Fig. 9. Schematic illustration of the germanium electrodeposition stages as the processing is increased when realized on PS substrates (a) immediately after anodization and (b) after subsurface layer removal.

alleviating diffusion limitations otherwise prevalent in freshly-prepared porous layers.

In addition to oxide removal, immersing the PS sample in HF prior to germanium electrodeposition ensures hydrogen passivation of the pore sidewalls that provides an increased degree of surface reactivity compared to the that of the untreated partially oxidized surface. Although the exposure time is not critical for hydrogen passivation of one given surface, it is of great importance in the case of processing a porous material and should be extensive enough to allow the acid to penetrate to the bottom of the pores. Excessive HF exposure time does not have any negative effect on the processing result. Deposition of germanium into the sample with insufficient or lacking HF preprocessing results in predominantly surface and near-surface germanium deposition due to the presence of SiO_2 at the sidewalls and bottoms of the pore channels.

Thermal processing of PS uniformly filled with germanium results in the formation of silicon-germanium alloy layers. Presumably, varying the geometric parameters of the initial PS layer will enable direct control over the resulting alloys' elemental composition, making it a relatively simple and reproducible method of forming Si-Ge alloys featuring desired compositions and thicknesses.

Declaration of Competing Interest

The authors declare that they have no known competing financial interests or personal relationships that could have appeared to influence the work reported in this paper.

Acknowledgments

We would like to thank D. Zhigulin (State Center "Belmicroanalysis", Affiliate Research & Design Center "Belmicrosystems", JSC "INTEGRAL", Minsk, Belarus) for performing SEM and EDX analyses of the experimental samples.

Funding

This research was financially supported by the Russian Science Foundation (Project No. 20-19-00720).

References

[1] Y. Peng, L. Miao, J. Gao, C. Liu, M. Kurosawa, O. Nakatsuka, S. Zaima, Realizing high thermoelectric performance at ambient temperature by ternary alloying in polycrystalline $Si_{1-x-y}Ge_xSn_y$ thin films with boron ion implantation, Sci. Rep. 9 (2019) 14342, doi:10.1038/s41598-019-50754-4.

[2] R. Basu, S. Bhattacharya, R. Bhatt, M. Roy, S. Ahmad, A. Singh, M. Navaneethan, Y. Hayakawa, D. Aswal, S. Gupta, Improved thermoelectric performance of hot pressed nanostructured n-type SiGe bulk alloys, J. Mater. Chem. A 2 (2014) 6922–6930, doi:10.1039/c3ta14259k.

[3] V.A. Volodin, G.K. Krivyakin, A.V. Bulgakov, Y. Levy, J. Beranek, S. Nagisetty, Z. Bryknar, N.M. Bulgakova, P.V. Geydt, A.A. Popov, Picosecond infrared laser crystallization of Ge layers in Ge/Si multinanolayers for optoelectronic applications, Proc. SPIE 12157 (2022) 1215702, doi:10.1117/12.2622731.

[4] A. Lahiri, S.Z. El Abedin, F. Endres, UV-assisted electrodeposition of germanium from an air- and water-stable ionic liquid, J. Phys. Chem. C 116 (2012) 17739–17745, doi:10.1021/jp3062543.

[5] X. Liu, J. Zhao, J. Hao, B. Su, Y. Li, 3D ordered macroporous germanium fabricated by electrodeposition from an ionic liquid and its lithium storage properties, J. Mater. Chem. A 1 (2013) 15076–15081, doi:10.1039/c3ta12923c.

[6] M. Wu, N. Brooks, S. Schaltin, K. Binnemans, J. Fransaer, Electrodeposition of germanium from the ionic liquid 1-butyl-1-methylpyrrolidinium dicyanamide, Phys. Chem. Chem. Phys. 15 (2013) 4955–4964, doi:10.1039/c3cp44554b.

[7] M. Wu, G. Vanhoutte, N. Brooks, K. Binnemans, J. Fransaer, Electrodeposition of germanium at elevated temperatures and pressures from ionic liquids, Phys. Chem. Chem. Phys. 17 (2015) 12080–12089, doi:10.1039/c4cp06076h.

[8] I.M. Gavrilin, Y.O. Kudryashova, A.A. Kuz'mina, T.L. Kulova, A.M. Skundin, V.V. Emets, R.L. Volkov, A.A. Dronov, N.I. Borgardt, S.A. Gavrilov, High-rate and low-temperature performance of germanium nanowires anode for lithium-ion batteries, J. Electroanal. Chem. 888 (2021) 115209, doi:10.1016/j.jelechem.2021.115209.

[9] X. Zou, L. Ji, Z. Pang, Q. Xu, X. Lu, Continuous electrodeposition of silicon and germanium micro/nanowires from their oxides precursors in molten salt, J. Energy Chem. 44 (2020) 147–153, doi:10.1016/j.jechem.2019.09.016.

[10] C. Fink, V. Dokras, Electrodeposition and electrowinning of germanium, J. Electrochem. Soc. 95 (1949) 80–97, doi:10.1149/1.2776740.

[11] X. Liang, Y. Kim, D. Gebergziabiher, J. Stickney, Aqueous electrodeposition of Ge monolayers, Langmuir 26 (2009) 2877–2884, doi:10.1021/la902929j.

[12] N. Chandrasekharan, S. Sevov, Anodic electrodeposition of germanium films from ethylenediamine solutions of deltahedral Ge_9^{4-} zintl ions, J. Electrochem. Soc. 157 (2010) 140–145, doi:10.1149/1.3309726.

[13] J. Ke, P. Bartlett, D. Cook, T. Easun, M. George, W. Levason, G. Reid, D. Smith, W. Su, W. Zhang, Electrodeposition of germanium from supercritical fluids, Phys. Chem. Chem. Phys. 14 (2012) 1517–1528, doi:10.1039/c1cp22555c.

[14] C. Cummings, P. Bartlett, D. Pugh, G. Reid, W. Levason, M. Hasan, A. Hector, J. Spencer, D. Smith, S. Marks, R. Beanland, Electrodeposition of protocrystalline germanium from supercritical difluoromethane, ChemElectroChem 3 (2016) 726–733, doi:10.1002/celc.201500539.

[15] Y. Uchida, T. Funayama, Y. Kogure, K. Ueno, Properties of electrodeposited germanium thin films, Phys. Status Solidi C 11 (2014) 1661–1664, doi:10.1002/pssc.201400094.

[16] Y. Uchida, T. Funayama, Y. Kogure, W. Yeh, Low-temperature Cu-induced polycrystallization of electrodeposited germanium thin film on flexible substrate, Phys. Status Solidi C 13 (2016) 864–867, doi:10.1002/pssc.201600140.

[17] Q. Cheek, E. Fahrenkrug, S. Hlynchuk, D. Hein Alsem, N. Salmon, S. Maldonado, *In situ* transmission electron microscopy measurements of ge nanowire synthesis with liquid metal nanodroplets in water, ACS Nano 14 (2020) 2869–2879, doi:10.1021/acsnano.9b06468.

[18] I.M. Gavrilin, D.G. Gromov, A.A. Dronov, S.L Dubkov, R.L. Volkov, A.Y. Trifonov, N.I. Borgardt, S.A. Gavrilov, Effect of electrolyte temperature on the cathodic deposition of Ge nanowires on in and Sn particles in aqueous solutions, Semiconductors 51 (2017) 1067–1071, doi:10.1134/S1063782617080115.

[19] N. Grevtsov, E. Chubenko, V. Petrovich, V. Bondarenko, I. Gavrilin, A. Dronov, S. Gavrilov, Selective electrochemical deposition of indium in-between silicon nanowire arrays fabricated by metal-assisted chemical etching, Materialia 21 (2022) 101337, doi:10.1016/j.mtla.2022.101337.

[20] I.M. Gavrilin, N.L. Grevtsov, A.V. Pavlikov, A.A. Dronov, E.B. Chubenko, V.P. Bondarenko, S.A. Gavrilov, A new approach for producing of film structures based on Si1-xGex, Mater. Lett. 313 (2022) 131802, doi:10.1016/j.matlet.2022.131802.

[21] A. Dolgiy, S. Redko, H. Bandarenka, S. Prischepa, K. Yanushkevich, P. Nenzi, M. Balucani, V. Bondarenko, Electrochemical deposition and characterization of ni in mesoporous silicon, J. Electrochem. Soc. 159 (2012) 623–627, doi:10.1149/2.050210jes.

[22] H. Bandarenka, V. Petrovich, O. Komar, P. Nenzi, M. Balucani, V. Bondarenko, Characterization of copper nanostructures grown on porous silicon by displacement deposition, ECS Trans. 41 (2012) 13–22, doi:10.1149/1.4711400.

[23] M. Haeri, M. Haeri, ImageJ plugin for analysis of porous scaffolds used in tissue engineering, J. Open Res. Softw. 3 (2013), doi:10.5334/jors.bn.

[24] J.M. Buriak, Organometallic chemistry on silicon and germanium surfaces, Chem. Rev. 102 (2002) 1272–1308, doi:10.1021/cr000064s.

[25] M. Shao, H. Wang, Y. Fu, J. Hua, D. Ma, Surface functionalization of HF-treated silicon nanowires, J. Chem. Sci. 121 (2009) 323–327, doi:10.1007/s12039-009-0037-4.

[26] O. Chyan, J. Chen, J. Wu, S. Chien, M. Liu, Discrete metal deposition on hydrogen terminated silicon surfaces: kinetics, morphologies and sensor applications, Mater. Res. Soc. Symp. Proc. 451 (1997) 267–273, doi:10.1557/PROC-451-267.

[27] R. Boukherroub, Chemical reactivity of hydrogen-terminated crystalline silicon surfaces, Curr. Opin. Solid State Mater. 9 (2005) 66–72, doi:10.1016/j.cossms.2006.03.006.

[28] A.I. Manilov, V.A. Skryshevsky, Hydrogen in porous silicon — a review, Mater. Sci. Eng. B 178 (2013) 942–955, doi:10.1016/j.mseb.2013.05.001.

[29] K.A. Perrine, A.V. Teplyakov, Reactivity of selectively terminated single crystal silicon surfaces, Chem. Soc. Rev. 39 (2010) 3256–3274, doi:10.1039/B822965C.

[30] A. Chenna, L. Hamadou, N. Benbrahim, A. Kadri, S. Boudinar, J. Electroanal. Chem. 802 (2017) 118–122, doi:10.1016/j.jelechem.2017.08.053.